Korean J. Chem. Eng., 37(2), 307-321 (2020)
DOI: 10.1007/s11814-019-0426-4

pISSN: 0256-1115
eISSN: 1975-7220

Thin film composite polyesteramide nanofiltration membranes fabricated from carboxylated chitosan and trimesoyl chloride

Dihua Wu*,†,‡, Xiru Zhang,‡, Yujie Chen*, Sanchuan Yu**,†, and Hongting Zhao***

*College of Materials and Environmental Engineering, Hangzhou Dianzi University, Hangzhou, China
**Key Laboratory of Advanced Textile Materials and Manufacturing Technology of Education Ministry, Zhejiang Sci-Tech University, Hangzhou, China
(*Received 11 July 2019 • accepted 10 November 2019*)

Abstract−Thin film composite polyesteramide nanofiltration membranes were fabricated with interfacial polymerization from carboxylated chitosan and trimesoyl chloride on a microporous polysulfone support membrane. Salt rejection was improved by building a multiple-layer structure that was formed by sequentially repeating the cycles of the interfacial reactions. The chemical structure, surface morphology and charge were characterized for the polyesteramide top layer. The effects of the concentrations of the reactant solutions and the number of cycles of reactant depositions and reactions on the separation performance were investigated. The single-layer polyesteramide membrane produced from 3.5 wt% carboxylated chitosan and 0.7 wt% TMC has a negatively charged surface and shows favorable separation performance: pure water permeation flux of 7.3 L/(m^2 h) at 0.6 MPa gauge feed pressure, and salt rejection of 95.0% for Na_2SO_4, 65.7% for $MgSO_4$, 33.2% for $MgCl_2$ and 66.3% for NaCl. The multiple-layer polyesteramide membranes show a more negatively charged surface and higher salt rejection than the single-layer polyesteramide membranes. The single-layer polyesteramide membrane PS-[(C-CS)$_{1.0}$/TMC] with a relatively loose structure shows good retention for the reactive black 5 anionic dye. This study opens an interesting research area to explore a new type of thin film composite nanofiltration membrane.

Keywords: Polyesteramide, Carboxylated Chitosan, Interfacial Polymerization, Thin Film Composite, Nanofiltration

INTRODUCTION

Nanofiltration (NF) membranes have high retention of divalent ions and organic molecules with relatively high flux and energy efficiency. Thus, NF has been applied in water softening [1], organic matter removal [2], biochemistry [3], pharmaceuticals [4], food [5] and dyeing [6]. Thin film composite (TFC) NF membranes with a selective skin layer on top of a porous substrate are predominantly used in the industry due to their high flux. The ultrathin skin layer, which is the key to good separation performance of a TFC membrane, is mostly composed of cross-linked polyamide (PA) prepared through interfacial polymerization. Piperazine (PIP) is the most commonly used monomer in the aqueous phase for interfacial polymerization. Tremendous research has focused on exploiting new monomers, such as 1,4-diaminocyclohexane (DCH) [7], cyclen [8] and 2,20-bis(1-hydroxyl-1-trifluoromethyl-2,2,2-trifluoroethyl)-4,40-methylenedianiline (BHTTM) [9], to enhance the performance of TFC NF membrane. Incorporation of inorganic nanoparticles into the barrier layer, e.g., zeolitic imidazolate framework (ZIF) nanoparticles [10] and attapulgite nanorods [11], has attracted intense interest in the effort to obtain high flux or improved antifouling properties. The process of interfacial polymerization can also be optimized by using a catalyst [12], adding a cosolvent to the organic phase [13,14], or modifying the support membrane [13,14].

The polyamide skin layer consists of amine-based monomers, while the polyester barrier layer can be fabricated from polyphenols or polyols as water-soluble monomers. Bisphenol A (BPA) [15], triethanolamine (TEOA) [16] and pentaerythritol (PE) [17] are monomeric hydroxyl reagents that participate in interfacial polymerization. In recent years, the use of polymeric water-soluble reactants for membrane fabrication has attracted increasing interest. These molecules show lower reactivity than the small molecular reactants, making the reaction more controllable. The amine-based polymeric reactants include polyethylenimine (PEI) [18], polyvinylamine (PVAm) [19] and polyamidoamine (PAMAM) dendrimers [20]. The promising polymeric polyhydroxy compounds are hyperbranched polyester (HPEs) [21], sericin [22], tannic acid [23] and polydopamine [24]. Generally, the polyamide skin layer has a more cross-linked structure than the polyester skin layer due to the higher reactivity of the amine group compared to that of the hydroxyl group, resulting in the higher salt rejection of the polyamide TFC NF membranes. However, the polyester TFC NF membranes show improved antifouling performance due to the abundant hydroxyl groups (i.e., -OH) on the membrane surface [16]. In addition, there is no chlorine attack site (i.e., the amide bonds -CO-NH-) on the polyester skin layer, and hence, polyester membranes are expected to have an enhanced chlorine resistance.

It is thus interesting to obtain a TFC NF membrane that integrates the promising features of both the polyamide and polyester

†To whom correspondence should be addressed.
E-mail: dihuaw@hotmail.com, yuschn@163.com
‡The two authors contributed equally to this paper.

membranes. Chitosan is a natural hydrophilic polymer, containing both -NH_2 and -OH as a reaction site for interfacial polymerization. Therefore, the resultant membranes have both polyamide and polyester structures. In addition, chitosan has been increasingly used for separation membrane formation [25,26] because of its good permselectivity, solvent stability and good film forming properties. Carboxylated chitosan is the product of chitosan carboxylation with the substituents of alkyl-carboxyl (i.e., R-COOH) group on the amino or/and hydroxyl sites of the chitosan molecules. On the one hand, the amine (-NH_2) and hydroxyl (-OH) groups are still present in the carboxylated chitosan molecules, and these groups can react with acyl chloride (-COCl) to form polyamide (-CO-NH-) or polyester (-CO-OR-) crosslinks. On the other hand, carboxylated chitosan is water soluble, which is an important property for its use as an aqueous reactant for interfacial polymerization. Chitosan is mainly soluble in aqueous medium in the presence of acid, which is unfavorable for interfacial polymerization because the byproduct of this reaction is generally HCl. Thus, an acidic environment will restrict the reaction from proceeding to completion, leading to a low cross-linking degree of the skin layer and poor separation performance for the membrane. The derived water-soluble carboxylated chitosan remedies the limitation of chitosan. Thus, it is a promising candidate aqueous reactant for interfacial polymerization. In addition, carboxylated chitosan with a macromolecular structure can be deposited on the surface of the support membrane rather than snake through the pores like a small molecular reactant. Good adhesion is obtained between the supramolecular chitosan and the substrate through noncovalent interactions. As mentioned, the relatively low reactivity of the polymeric reactant makes it easier to control the interfacial polymerization, providing greater flexibility in the tailoring of the membrane properties. Therefore, in the present study, the aqueous phase and organic phase reactants were composed of carboxylated chitosan and trimesoyl chloride (TMC), respectively. Single-layer and multiple-layer polyesteramide membranes were prepared by once and sequential interfacial polymerizations, respectively. These membranes have several advantages: (1) they contains both polyamide and polyester links that can integrate the advantages of polyamide membrane (high salt rejection) and polyester membrane (high surface hydrophilicity); (2) the membrane properties can be tailored by adjusting the number of polyesteramide layer. Therefore, an interesting research area has been opened to prepare and tailor the polyesteramide TFC membranes. The effects of the reactant concentrations and the number of cycles of interfacial polymerization on the separation performance were studied. The surface properties of the skin layer (chemical composition, surface morphology, roughness, hydrophilicity and charge) were characterized by attenuated total reflection Flourier transformed infrared spectroscopy (ATR-FTIR), field emission scanning electron microscopy (FE-SEM), atomic force microscopy (AFM), contact angle and streaming zeta potential, respectively. Four salt solutions (Na_2SO_4, $MgSO_4$, $MgCl_2$ and NaCl) were used as representatives to evaluate the membrane performance. Furthermore, the dye removal efficiency of polyesteramide NF was tested using indigo carmine, reactive black 5 and rhodamine B. The effects of the feed dye concentrations and operating pressures on the dye removal efficiency were also investigated.

EXPERIMENTAL

1. Materials

The flat-sheet polysulfone (PS) substrate with a water permeability of ~120 L/m^2 h bar, and molecular weight cut-off (MWCO) of ~100,000 g/mol was supplied by Hangzhou Tianchuang Environmental Technology Co., LTD., China. Carboxylated chitosan,

Table 1. Information about the dyes used in the study

Name	Molecular formula	Molecular weight (g/mol)	Detection wavelength (nm)	Molecular structure
Indigo carmine	$C_{16}H_8N_2Na_2O_8S_2$	466	610	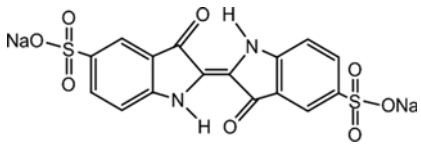
Reactive black 5	$C_{26}H_{21}N_5Na_4O_{19}S_6$	992	599	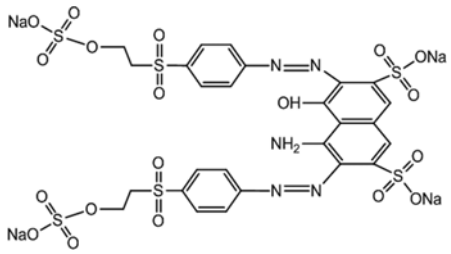
Rhodamine B	$C_{28}H_{31}ClN_2O_3$	479	554	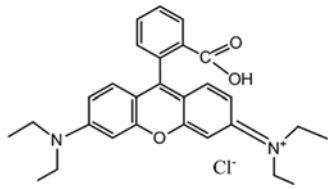

trimesoyl chloride, hexane, Na_2SO_4, $MgCl_2$, $MgSO_4$, NaCl, indigo carmine and rhodamine B were purchased from Shanghai Macklin Biochemical Co., Ltd. Reactive black 5 was purchased from Sigma-Aldrich. The details for the dyes used in this study are presented in Table 1. All these chemicals were reagent grade and were used without any further purification.

2. Membrane Preparation

Based on the similarity-intermiscibility theory, a predetermined amount of carboxylated chitosan (0.5-3.0 wt%) was dissolved in deionized water to prepare the aqueous phase reactant solution, and TMC (0.1-0.7 wt%) was dissolved in hexane to obtain the organic phase reactant solution. The PS substrate membrane was soaked in deionized water overnight in advance, and the preservatives on the surface were removed by washing the membrane thoroughly with deionized water. The water wet PS was dried in air and then clamped between two Teflon frames with a height of 1.2 cm and a circular inner cavity with a diameter of 7 cm. The carboxylated chitosan solution was charged into the top of the substrate and contacted with the surface of the PS substrate for 15 min, and the excess aqueous solution was removed. The reactant-loaded PS membrane was dried by positioning the frame holder on the top and bottom edges in air for 30 min. The TMC solution was then poured on top of the carboxylated-chitosan-loaded membrane and contacted for 15 min to carry out the interfacial polymerization on the surface of the substrate. A heat treatment was taken at 55 °C for 20 min for the membrane after removing the excess TMC solution, which appeared to be moderate values of temperature and duration time for heat treatment based on the reported literatures for developing nanofiltration membranes [18, 22-24]. The formed membrane was rinsed thoroughly with deionized water and stored in the deionized water prior to the NF test. The chemical structure of PS is shown in Fig. 1(a) and the interfa-

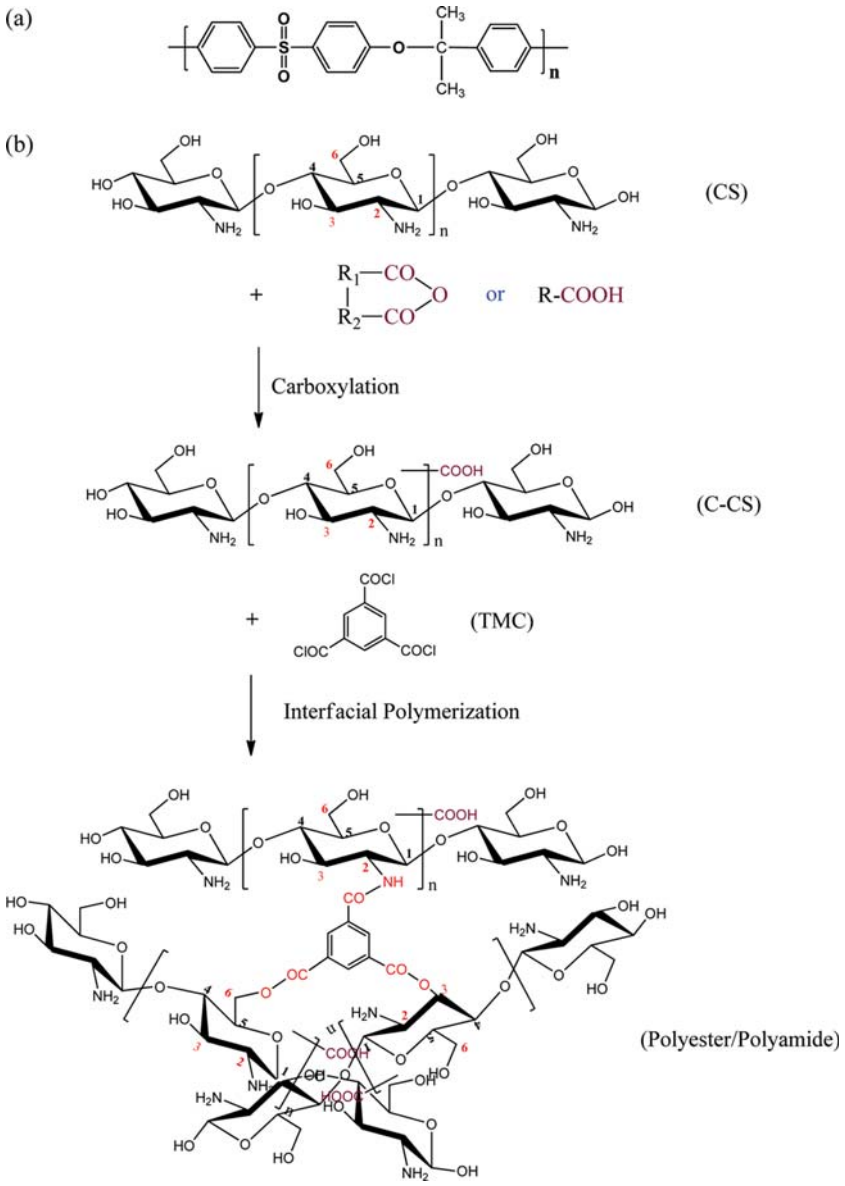

Fig. 1. Chemical structure of polysulfone (a) and interfacial reaction between carboxylated chitosan and TMC (b).

Table 2. Membrane designation based on the reactant concentration and the number of reactant depositions

Type of polyesteramide layer	Number of reactant depositions	Membrane designation	Description
Single	2	PS-[(C-CS)$_n$/TMC]	Single-layer polyesteramide membrane formed by interfacial polymerization between carboxylated chitosan and TMC; "n" is the concentration of carboxylated chitosan
Multiple	1	PS-(C-CS)	PS support membrane deposited with carboxylated chitosan
	2	PS-[(C-CS)/TMC]$_1$	Single-layer polyesteramide membrane formed by interfacial polymerization between carboxylated chitosan and TMC
	2n	PS-[(C-CS)/TMC]$_n$	Multiple-layer polyesteramide membrane with n interfacially polymerized layers formed by interfacial polymerization between carboxylated chitosan and TMC
	2n+1	PS-[(C-CS)/TMC]$_n$-(C-CS)	Membrane PS-[(C-CS)/TMC]$_n$ deposited with carboxylated chitosan

cial reaction between carboxylated chitosan and TMC to form a polyesteramide cross-link is illustrated in Fig. 1(b).

The multiple-layer polyesteramide was built up by repeating the interfacial polymerization, i.e., conducting the interfacial polymerization sequentially. For a clear demonstration, the membrane designations are shown in Table 2 according to the reactant concentrations and the number of reactant depositions. The composite membrane is designated based on one deposition layer after depositing the first aqueous reactant phase (PS-(C-CS)), based on two deposition layers after depositing the second organic reactant phase (PS-[(C-CS)/TMC]), and so on in a similar manner. Considering the accumulative mass transfer resistance generated by the multiple layers, the concentrations of carboxylated chitosan and TMC were 1.0 wt% and 0.2 wt%, respectively. The contact time for the first aqueous phase reactant solution, the drying time for the aqueous phase reactant solution and the reaction time of each cycle of interfacial polymerization were the same as those used in the single-layer polyesteramide membrane formation. The membrane was finally treated at 55 °C for 20 min. There was no drying time for the organic phase reactant solution because hexane evaporated immediately after the solution was removed from the membrane surface. No other treatment, such as water rinsing, was performed between the interfacial polymerization cycles in order to retain the amount and activity of the residual unreacted functional groups.

3. Membrane Characterization

The chemical structure of the skin layer was characterized by ATR-FTIR (Nicolet Aratar 370 FTIR spectrometer). A ZnSe crystal at an incidence angle of 45° was used. For each sample, a resolution of 4 cm^{-1} and total scan of 32 was applied in the ATR-FTIR analysis.

The FE-SEM (HitachiS-4800, Japan) was used to investigate the surface morphology of the TFC membranes. The AFM (Park Scientific Instrument Autoprobe CT) was applied to examine the surface roughness of the membranes in the tapping mode. A 10 μm× 10 μm scan area was analyzed for each membrane sample, and root mean square roughness (RMS) was used to describe the surface roughness of the membranes.

The Anton Paar zeta potential analysis meter (Austria) was used for streaming potential measurements for investigating the surface charge of the membranes. The membrane sample was fixed in the measurement cell with a KCl solution (0.001 M, pH=2-11) circulation at 25 °C. At least three measurements were repeated and the average values were presented.

The DSA10-MK2 contact angle meter (KRUSS BmbH Co, Germany) was used to measure the surface hydrophilicity of the membrane. The contact angles were measured at 25 °C on the dried membrane surfaces by sessile drop method with deionized water (approximately 3 μL). The membrane samples were dried in air at room temperature before the contact angle measurements. At least six measurements at different surface locations were performed for each membrane sample, and the average values are reported here.

4. Salt Rejection and Dye Removal

The separation performance of the membranes was evaluated in terms of water flux and salt rejection, which were tested with a laboratory-scale cross-flow test unit. The effective permeation area for the membrane of a test cell is 23.6 cm^2. The membrane was conditioned for 1 h at 0.7 MPa gauge with deionized water and then the measurement of the permeation flux of pure water started under 0.6 MPa gauge, followed by the NF experiments for Na_2SO_4, $MgSO_4$, $MgCl_2$, and NaCl solutions at a salt concentration of 500 ppm and pH=7.0±0.2 in the feed. The water flux was evaluated in the units of L/(m^2 h) by testing the permeate flow directly. The salt rejection was calculated as rejection (%)=100×(1−(C_P/C_F)), where C_P and C_F are the permeate salt concentration and feed salt concentration, respectively. C_P and C_F were determined by testing the electrical conductivity of the solution.

Dye removal experiments were carried out with indigo carmine, reactive black 5 and rhodamine B under the feed concentrations of 50-1,500 ppm and operating pressures of 0.3-0.7 MPa. The dye concentrations of the aqueous solutions were measured using a Shimadzu UV-170 spectrophotometer at the maximum absorption wavelengths of the dyes.

The experimental error of flux, salt rejection and dye removal efficiency are within 2% in duplicate tests for a given membrane, while the variation of water flux is within 10% and that of salt rejec-

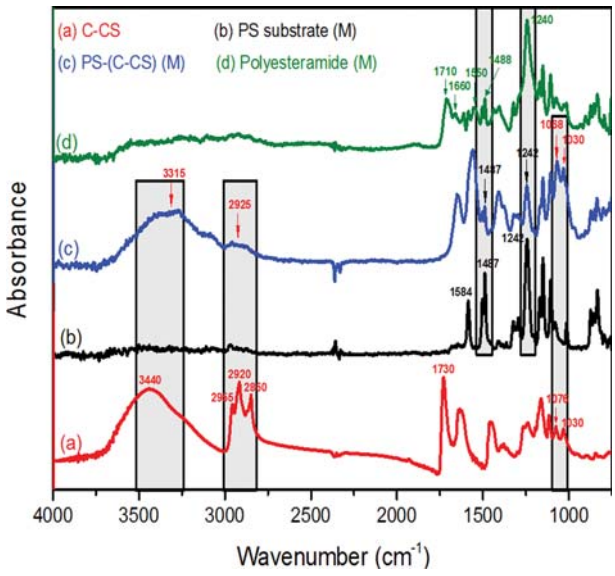

Fig. 2. FTIR spectra of (a) carboxylated chitosan, (b) PS substrate, (c) PS-(C-CS) composite membrane and (d) PS-[(C-CS)$_{2.0}$/TMC] composite membrane.

tion and dye retention is within 5% in the batch-to-batch measurements.

RESULTS AND DISCUSSION

1. Polyesteramide Layer Characterization

1-1. Chemical Structure

Fig. 2 shows the FTIR spectra of the carboxylated chitosan, PS substrate, carboxylated chitosan loaded membrane (PS-(C-CS) membrane) and the single-layer polyesteramide composite membrane. The assignments of the characteristic bands are shown in Table 3. The bands of N-H stretching at 3,315 cm^{-1}, C-H stretching at 2,925 cm^{-1}, and C-O stretching at 1,068 and 1,030 cm^{-1} on the PS-(C-CS) membrane indicate that carboxylated chitosan was well-anchored on the PS substrate. The new bands appearing at 1,710, 1,660 and 1,550 cm^{-1} suggest that ester and amide bounds were formed on the membrane surface.

1-2. Surface Charge and Hydrophilicity

The zeta potentials tested at different pH for the single-layer and multiple-layer polyesteramide layers membrane are shown in Figs. 3(a) and 4(a), and the isoelectric points for these two series of membranes are shown in Figs. 3(b) and 4(b), respectively. The isoelectric points of these two series of membranes are both lower than 4, which means that the surface is negatively charged at the testing conditions of NF performance (pH=6.8-7.2). It is known that the composite membrane with a chitosan coating top layer is positively charged because of the primary amine (-NH_2) group on the surface [27]. However, the carboxylation process introduced the carboxyl group (-COOH) into the chitosan molecules by the substitution reactions of -NH_2 on the C_2 positions, and of hydroxyls (-OH) on the C_3 and C_6 positions of the original chitosan [28]. The amount of the introduced -COOH exceeds that of the remaining -NH_2. Thus, the membrane with only one reactant deposition, PS-(C-CS) membrane, is negatively charged.

For the single-layer polyesteramide membranes, the membrane is negatively charged because of the dissociation of the carboxylic acid groups caused by partial hydrolysis of the acyl chloride unit (-COCl) of TMC on the membrane surface [29]. However, the isoelectric point varies in a very small range (within 0.2) with an increase of the reactant concentration of carboxylated chitosan. This occurs because the -NH_2/-COOH ratio remained the same even though the number of both the -NH_2 and -COOH groups increased with increasing concentration of carboxylated chitosan in the aque-

Table 3. Band assignments for the infrared spectra

Materials	Wavenumber (cm^{-1})	Assignment
Caboxylated chitosan	~3340	ν(N-H), ν(O-H)
	2955, 2920, 2850	ν(C-H) from -CH_3 or -CH_2
	1730	ν(C=O) from -COOH
	1076	ν(C-O) from C_3-OH
	1030	ν(C-O) from C_6-OH
PS substrate	1584	Benzene rings
	1487	ν(C=C)
	1242	Aromatic ether
PS-(C-CS) membrane	~3315	ν(N-H), ν(O-H)
	~2925	ν(C-H) from -CH_3 or -CH_2
	1487	ν(C=C)
	1242	Aromatic ether
	1068	ν(C-O) from C_3-OH
	1030	ν(C-O) from C_6-OH
Single-layer polyesteramide membrane	1710	ν(C=O) from ester group
	1660	Amide I, ν(C=O)
	1550	Amide II, δ(N-H) bending

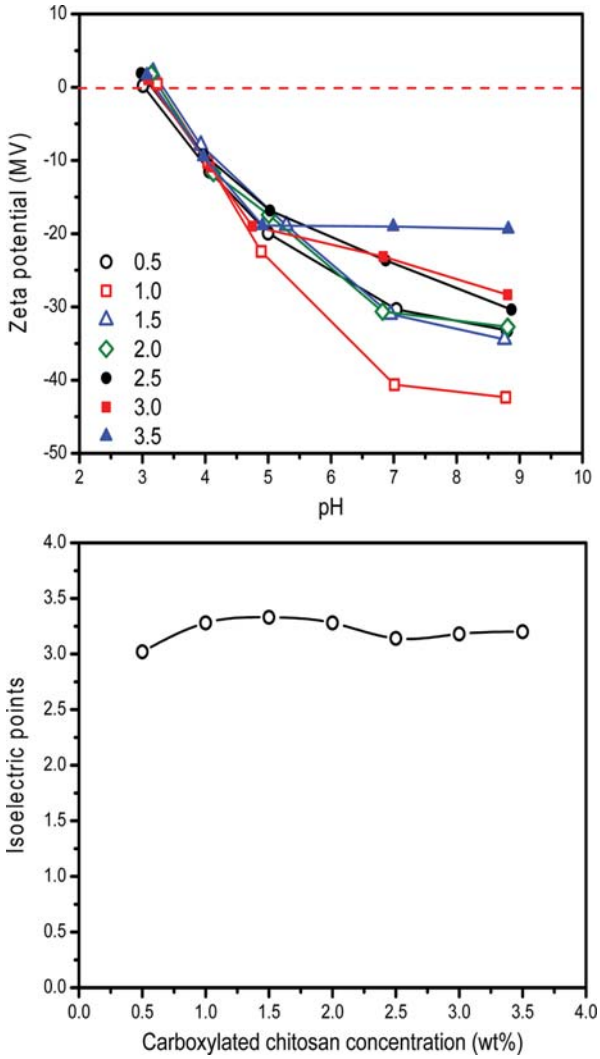

Fig. 3. Zeta potential at different pH values (a) and isoelectric point (b) for single-layer polyesteramide membranes. Test at 25 °C with 0.001 M KCl.

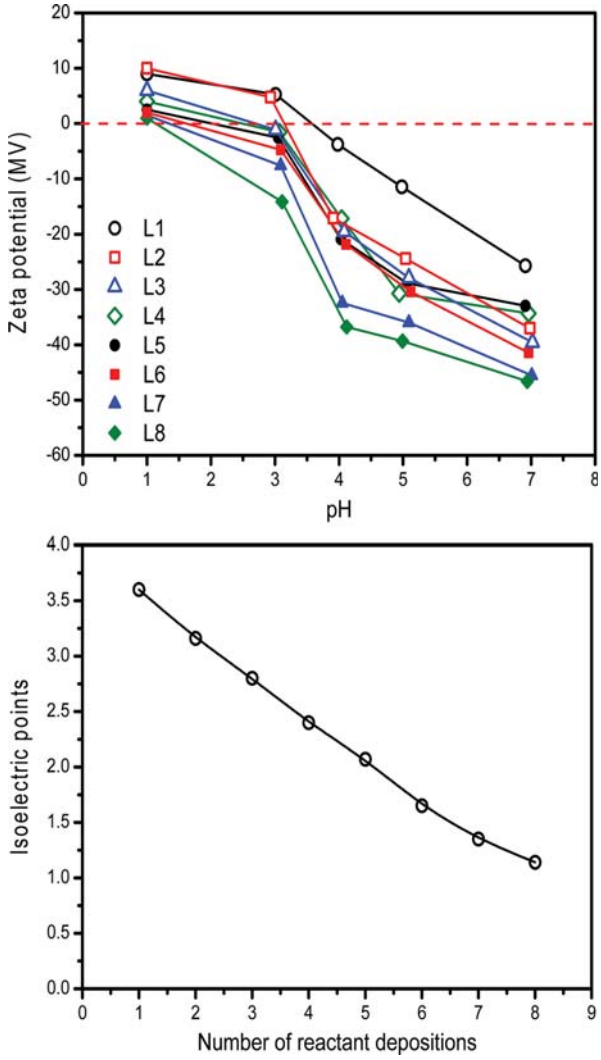

Fig. 4. Zeta potential at different pH values (a) and (b) isoelectric point for multiple-layer polyesteramide membranes. Test at 25 °C with 0.001 M KCl.

ous solutions. In addition, the concentration ratio of carboxylated chitosan and TMC was fixed at a moderate value of 5 : 1 [22-24]. Therefore, it is assumed that the reaction degree remains the same in the entire reactant concentration range, resulting in a constant ratio of -NH_2/-COOH on the membrane surface. For the multiple-layer polyesteramide membranes, the isoelectric point continuously decreases with increasing reactant concentration. The multiple-layer polyesteramide membrane was formed by repeating the interfacial reaction sequentially. The reaction degree becomes lower with additional interfacial polymerization cycles, resulting in more residual acyl chloride units (-COCl) from TMC. The hydrolysis of these residua acyl chloride unit (-COCl) produces more carboxylic acid groups and causes the gradually decreased isoelectric point. The polyelectrolyte multilayer nanofiltration membranes terminated with a polyanion layer also shows a more negatively charged surface by increasing the number of anionic polyelectrolyte deposition [30,31].

Fig. 5 shows the water contact angles of the two-series compos-

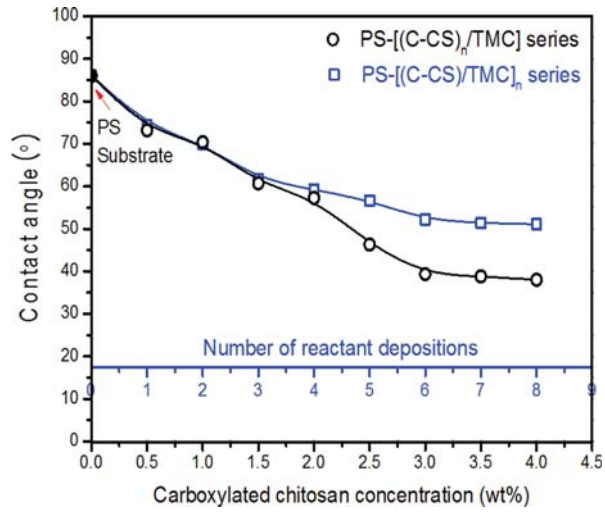

Fig. 5. Water contact angle varies with the reactant concentration and number of reactant depositions.

ite polyesteramide membranes. It is observed that the membrane surface hydrophilicity is improved by increasing either the reactant concentration or the number of reactant depositions, with a slightly better effect of the former than the latter. Note that the volume of the reactant solution remained the same for every deposition, both in the single-layer and multiple-layer polyesteramide membrane formation. The concentration of the carboxylated chitosan used for the multiple-layer polyesteramide membrane formation remained unchanged at 1.0 wt% in every interfacial polymerization cycle. Therefore, the total amount of the reactants used

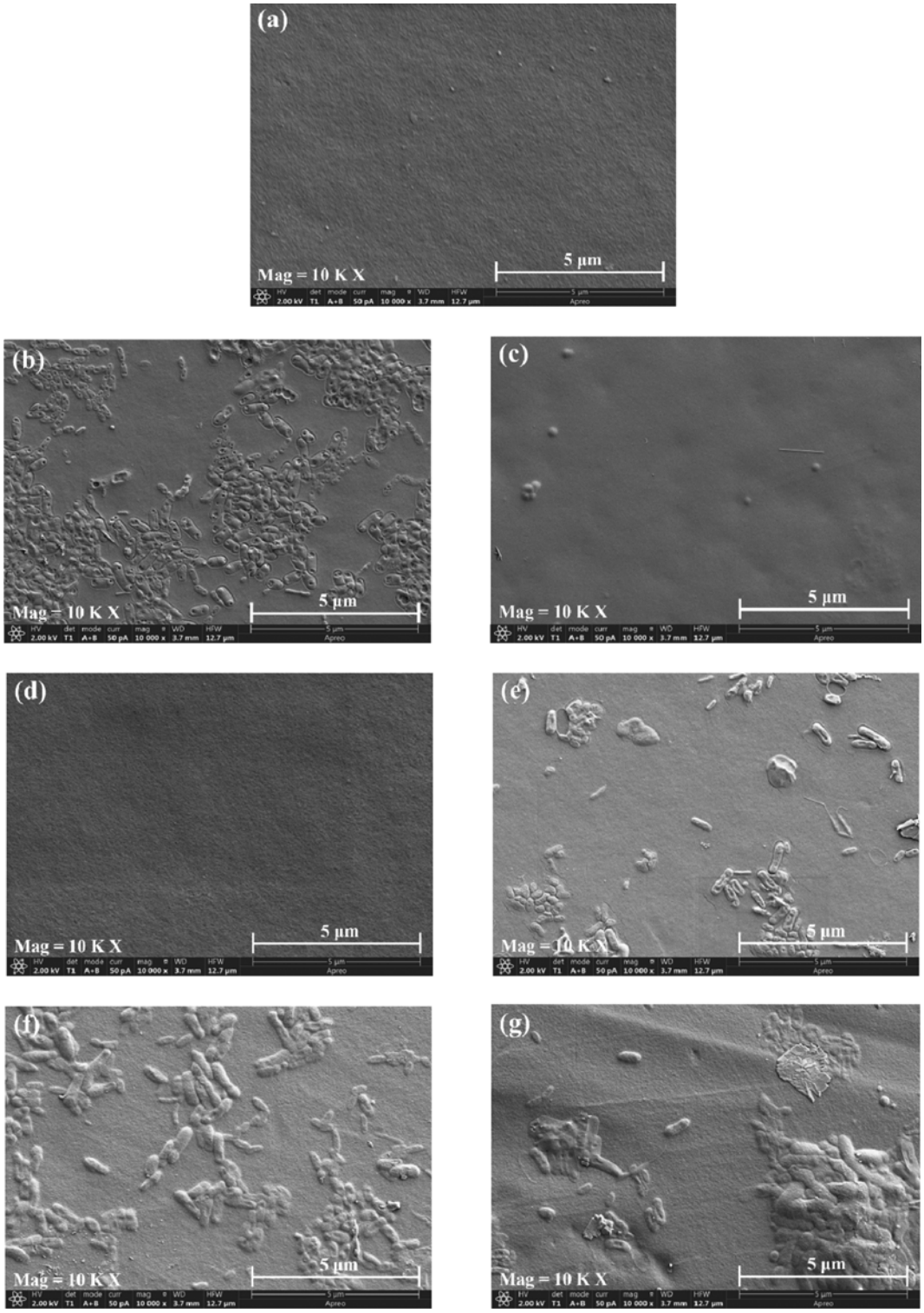

Fig. 6. Surface images (10,000×) of (a) PS support membrane, (b) membrane PS-[(C-CS)$_{1.5}$/TMC], (c) membrane PS-[(C-CS)$_{3.0}$/TMC], (d) membrane PS-(C-CS), (e) membrane PS-[(C-CS)/TMC]$_1$, (f) membrane PS-[(C-CS)/TMC]$_1$-(C-CS) and (g) membrane PS-[(C-CS)/TMC]$_2$.

to form the multiple-layer polyesteramide membrane with the number of reactant depositions of "2n" (i.e., "n" polyesteramide layer) is the same as that used to form the single-layer polyesteramide membrane from the carboxylated chitosan concentration of "n" wt%. For example, the membranes PS-$[(C\text{-}CS)/TMC]_1$ and PS-$[(C\text{-}CS)_{1.0}/TMC]$ consume the same amount of carboxylated chitosan and TMC during the membrane preparation. However, for the membranes with multiple-layer structures, the hydrophilic groups, e.g., $-NH_2$, -COOH and -OH, on the bottom layers are probably covered by the top layers. Hence, fewer hydrophilic groups emerged on the membrane surface, resulting in a relatively lower apparent hydrophilicity.

1-3. Surface Morphology

Surface images of the PS support membrane and the composite polyesteramide membranes are shown in Fig. 6. It is observed that the PS substrate is plain and smooth with very few pores and granular particles on the surface, while the composite polyesteramide membrane exhibits a quite different morphology. Many nodules are observed on the PS-$[(C\text{-}CS)_{1.5}/TMC]$ membrane resulted from the cross-linking structure of formed polyesteramide [24]. However, the PS-$[(C\text{-}CS)_{3.0}/TMC]$ membrane becomes smooth again. It is known that the reactivity of $-NH_2$ is higher than that of -OH, so that the cross-linking degrees of the polyamide and polyester networks are different, leading to the unevenness of the membrane surface. By increasing the reactant concentration, the cross-linking degrees of both polyamide and polyester networks are enhanced. Meanwhile, the difference between the polyamide and polyester can be compensated for by the excess carboxylated chitosan with a macromolecular structure on the membrane surface. In addition, the polymeric molecules carboxylated chitosan in aqueous phase hardly diffuse into the organic phase, then TMC will diffuse into the aqueous/organic interface to react with carboxylated chitosan. The depth of reaction will be limited and the formed layer will be smooth and thin. Therefore, it is not surprising that the surface of PS-$[(C\text{-}CS)_{3.0}/TMC]$ appears as smooth as that of the PS substrate, but the composite membrane is denser than the support membrane due to the deposition of the polyesteramide layer. Zhou et al. [22] and Zhang et al. [23] observed the same results. For the multiple-layer polyesteramide series membrane, the membrane with only one carboxylated chitosan deposition, membrane PS-(C-CS), displays an even smoother surface than the support membrane, suggesting that the carboxylated chitosan macromolecules can be distributed evenly on the membrane surface. By depositing the organic reactant solution and further increasing the number of interfacial polymerization cycles, more nodules appear on the membrane surface. The nodules are likely to aggregate when there are four reactant depositions on the membrane surface. The cross-sectional images of the single-layer polyesteramide membrane PS-$[(C\text{-}CS)/TMC]_1$ and multiple-layer polyesteramide membrane PS-$[(C\text{-}CS)/TMC]_2$ are shown in Fig. 7. The PS substrate clearly shows a finger-like structure (see Part A in images) and spongy-like structure (see Part B in images). A very thin layer (see Part C in images), which is polyesteramide skin layer, can be observed on the top of PS substrate. The membrane PS-$[(C\text{-}CS)/TMC]_2$ has a

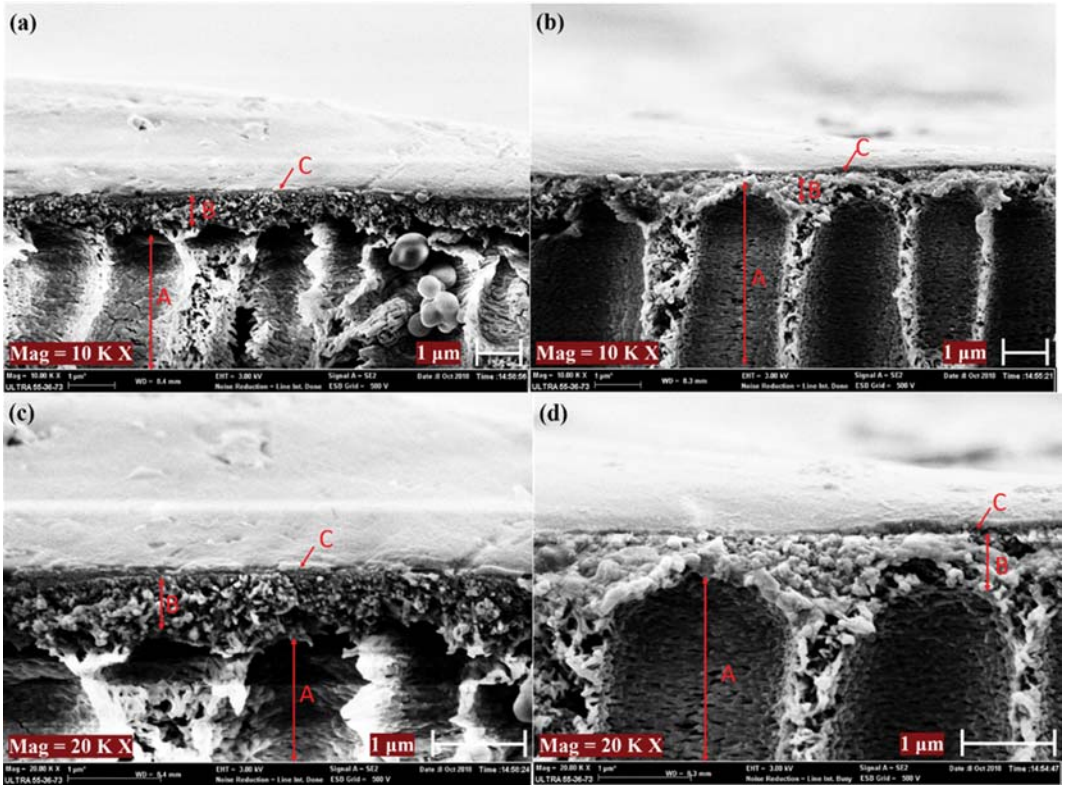

Fig. 7. Cross-sectional images (10,000×) of (a) membrane PS-$[(C\text{-}CS)/TMC]_1$, membrane (b) PS-$[(C\text{-}CS)/TMC]_2$ and (20,000×) of (a) membrane PS-$[(C\text{-}CS)/TMC]_1$, membrane (b) PS-$[(C\text{-}CS)/TMC]_2$.

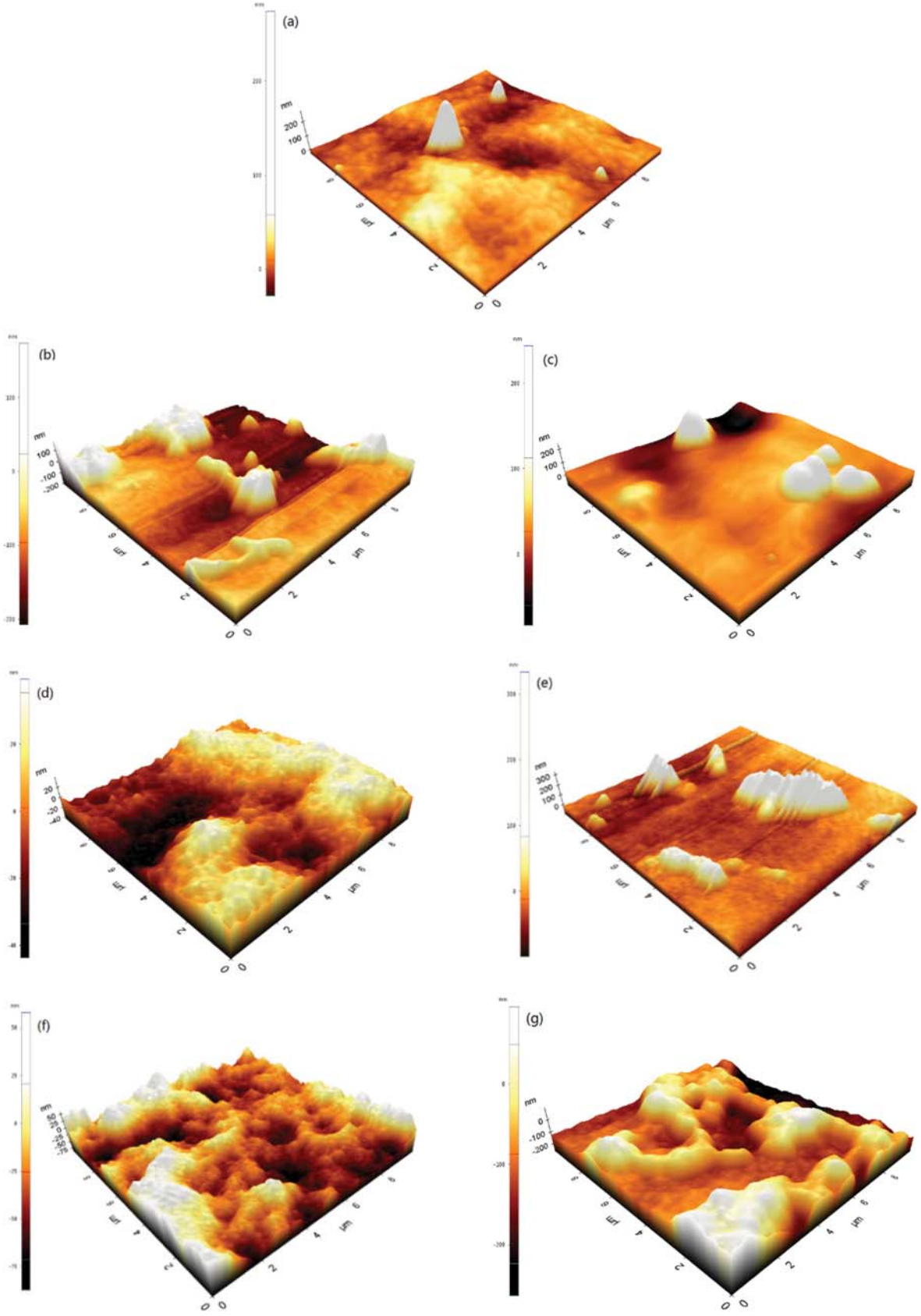

Fig. 8. AFM images (10 μm×10 μm) of (a) PS support membrane, (b) membrane PS-[(C-CS)$_{1.5}$/TMC], (c) membrane PS-[(C-CS)$_{3.0}$/TMC], (d) membrane PS-(C-CS), (e) membrane PS-[(C-CS)/TMC]$_1$, (f) membrane PS-[(C-CS)/TMC]$_1$-(C-CS) and (g) membrane PS-[(C-CS)/TMC]$_2$.

Table 4. Root mean square roughness of composite polyesteramide membranes

Membrane	PS	PS-[(C-CS)$_{1.5}$/TMC]	PS-[(C-CS)$_{3.0}$/TMC]	PS-(C-CS)	PS-[(C-CS)/TMC]$_1$	PS-[(C-CS)/TMC]$_1$-(C-CS)	PS-[(C-CS)/TMC]$_2$
Roughness (nm)	21.06	47.86	34.37	12.44	43.40	49.06	56.13

thicker top layer than the membrane PS-[(C-CS)/TMC]$_1$. The thickness of the single polyesteramide layer ([(C-CS)/TMC]$_1$) is estimated to be ~70 nm, which is a reasonable value of thickness for the skin layer of TFC membrane (60-300 nm) [32,33].

Fig. 8 shows a 10 μm×10 μm scan of the three-dimensional AFM images, and Table 4 presents the root mean square roughness data of the membrane. The AFM results coincide with the surface morphologies observed by SEM. It is observed that the small cone-shape structures are evenly distributed on the PS substrate, leading to a smooth surface with the roughness of 21.06 nm. The peak-valley structures that appear on the PS-[(C-CS)$_{1.5}$/TMC] membrane increase the surface roughness to 47.86 nm, while the roughness of the PS-[(C-CS)$_{3.0}$/TMC] membrane decreases to 34.37 nm due to the "filling up" effects caused by the excess carboxylated chitosan. The roughness of the PS-(C-CS) membrane is lower than that of the PS substrate, further confirming that the small unevenness of the PS substrate can be compensated by the carboxylated chitosan macromolecules. As the number of reactant depositions increases, the surface morphology first presents a peak-valley structure and then changes to a nodular aggregated structure, and the surface roughness of the membrane increases gradually.

2. Effects of the Membrane Fabrication Conditions on Separation Performance

2-1. Effects of the Concentration of Reactant Solution

The permeation flux and salt rejection of the single-layer polyesteramide membrane prepared from the carboxylated chitosan and TMC with different concentrations are shown in Fig. 9. As expected, with increasing concentration of the reactant solution, the permeation flux decreases and the salt rejection increases. The permeation flux of PS support membrane is relatively high, which is 355 L/(m^2·h) observed at 0.2 MPa gauge. It remains as high as ~110 L/(m^2·h) when the reactant concentration is 0.5 wt% for carboxylated chitosan and 0.1 wt% for TMC, while the salt rejections of the formed membrane appear relatively low (27.9% for Na_2SO_4, 23.2% for $MgSO_4$, 17.0% for $MgCl_2$ and 23.9% for NaCl). Increasing the concentration of carboxylated chitosan from 1.0 to 2.0 wt% (concentration of TMC from 0.2 to 0.4 wt%), the permeation flux of the membrane decreases to 48.3 L/(m^2·h), and the rejection of Na_2SO_4, $MgSO_4$, $MgCl_2$ and NaCl increases in a small range, from 61.5 to 66.1%, from 37.2 to 43.4%, from 24.5 to 30.9% and from 32.0% to 45.7%, respectively. With a further increase in the carboxylated chitosan concentration up to 3.5 wt% (concentration of TMC up to 0.7 wt%), the permeation flux of the membrane gradually decreases to 7.3 L/(m^2·h) and the rejection of Na_2SO_4 reaches to 95.0%. The rejection of $MgSO_4$, $MgCl_2$ and NaCl increases up to 65.7%, 33.2% and 66.3%, respectively.

It is understandable that the polymerization reaction proceeds slowly at a low reactant concentration, leading to a thin and loose structure of the skin layer. A thicker and more compact top layer will be obtained at a high reactant concentration. Consequently,

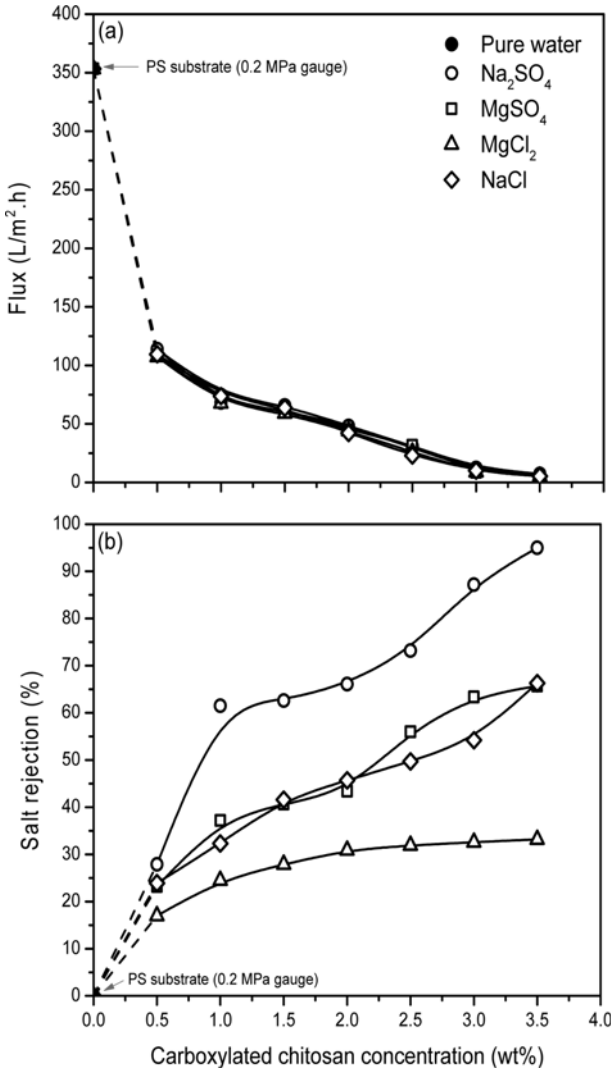

Fig. 9. Permeation flux (a) and salt rejection (b) of single-layer polyesteramide membranes vary with the reactant concentration (Testing conditions: 0.6 MPa gauge for polyesteramide membrane, 0.2 MPa gauge for PS support membrane, 500 ppm salt concentration, 25 °C).

the water flux declines and the salt rejection increases. The rejection of the four salts follows the order of Na_2SO_4>NaCl≈$MgSO_4$>$MgCl_2$. Similar results were observed for other polyester membranes [22]. The zeta potential measurements show that the membrane surface is negatively charged under the test conditions (pH= 6.5), so that the membrane preferentially rejects the salt of a multivalent anion and monovalent cation due to Donnan exclusion, leading to the highest rejection obtained for Na_2SO_4. The strong affinity between the membrane surface and the multivalent cation results in the lowest rejection of $MgCl_2$. In addition, the rejection

of NaCl is higher than that of $MgSO_4$ despite the smaller size of the former. This indicates that the electrostatic interactions between the membrane surface and the ionic feed solution are more important than the size sieving effects for the salt rejection.

2-2. Effects of Number of Reactants Depositions

The permeation flux and salt rejection of the multiple-layer polyesteramide membranes are shown in Fig. 10. Not surprisingly, the permeation flux decreases and the salt rejection increases with the additional interfacial polymerization cycles, because the skin layer becomes denser and thicker. For the membrane with four polyesteramide layers, the water flux decreases to 6.7 L/(m^2·h), and the rejection is 97.0% for Na_2SO_4, 67.4% for $MgSO_4$, 49.7% for $MgCl_2$ and 54.7% for NaCl. Unlike the single-layer polyesteramide membranes, this series of membranes has a higher rejection for $MgSO_4$ than NaCl. This is probably because the multiple-layer polyesteramide membranes have a more negatively charged surface than the single-layer polyesteramide membranes, resulting in a higher retention for the salt with the SO_4^{2-} divalent anion. The decrement of the permeation flux becomes smaller and finally levels off because the adsorption of the additional carboxylated chitosan macromolecules on the surface of the polymerized (C-CS)/TMC layer is less favorable than that on the PS surface.

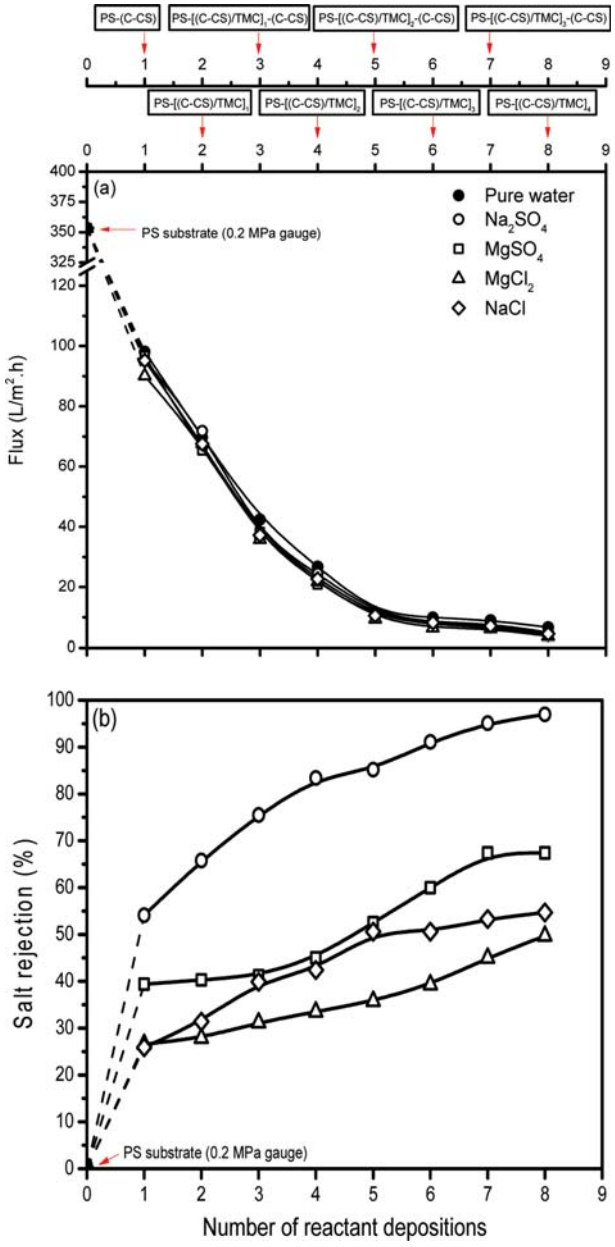

Fig. 10. Permeation flux (a) and salt rejection (b) of multiple-layer polyesteramide membranes vary with the number of reactant deposition (Testing conditions: 0.6 MPa gauge for polyesteramide membrane, 0.2 MPa gauge for PS support membrane, 500 ppm salt concentration, 25 °C).

As mentioned in Section 3.1.2, the PS-[(C-CS)$_n$/TMC] membrane and the PS-[(C-CS)/TMC]$_n$ membrane consume the same total amount of reactants when the volume of the reactant solution is the same for every deposition. The separation performance of the PS-[(C-CS)$_n$/TMC] series membranes and PS-[(C-CS)/TMC]$_n$ series membranes is compared in Fig. 11. The PS-[(C-CS)$_{1.0}$/TMC] membrane and the PS-[(C-CS)/TMC]$_1$ are the same membranes that were prepared from different batches, and therefore, they have similar permeation flux and salt rejection values. When the total amount of the reactants deposited on the membrane surface increases to a moderate range, the PS-[(C-CS)/TMC]$_2$ shows an obviously lower flux and higher rejection of Na_2SO_4 than the PS-[(C-CS)$_{2.0}$/TMC] membrane, which is presumably due to the accumulated thickness and negative charge of the multiple-layer polyesteramide membrane obtained during the sequential interfacial polymerization [30,31,34]. In addition, the relative lower hydrophilicity of PS-[(C-CS)/TMC]$_n$ series membranes (see Fig. 5) is presumably another reason for the lower flux. With a further increase in the total amount of the deposited reactants, the difference in the permeation and salt rejection between these two series of membranes decreases again. This is because the defects of the single polyesteramide layer have been healed by the large amount of reactant deposition. On the other hand, for the multiple-layer polyesteramide membrane, the additional carboxylated chitosan macromolecules become less favorably adsorbed on the surface of the formed polyesteramide. This indicates that at a given amount of reactant consumption, increasing the number of reactant depositions is more effective for enhancing the salt retention than increasing the concentration of the reactant, even though this effect becomes less significant with increasing amount of reactant consumption.

A comparison of the PS-[(C-CS)$_{3.5}$/TMC] and PS-[(C-CS)/TMC]$_4$ membranes with some other polyester membrane in terms of water permeability and salt rejections is shown in Table 5. The PS-[(C-CS)$_{3.5}$/TMC] and PS-[(C-CS)/TMC]$_4$ membranes show comparable flux and high salt rejections. It is feasible to fabricate an NF membrane with good separation performance by interfacial polymerization from carboxylated chitosan and TMC. In addition, the membranes show to be stable. The water flux and Na_2SO_4 rejection of a pristine PS-[(C-CS)$_{3.5}$/TMC] membrane is 7.3 L/(m^2 h) and 95%, respectively. The water flux and Na_2SO_4 rejection of this membrane is maintained as 7.2 L/(m^2 h) and 95% after extensive NF tests for over two weeks with the various salt solutions (Na_2SO_4, $MgSO_4$, $MgCl_2$ and NaCl) at different concentrations.

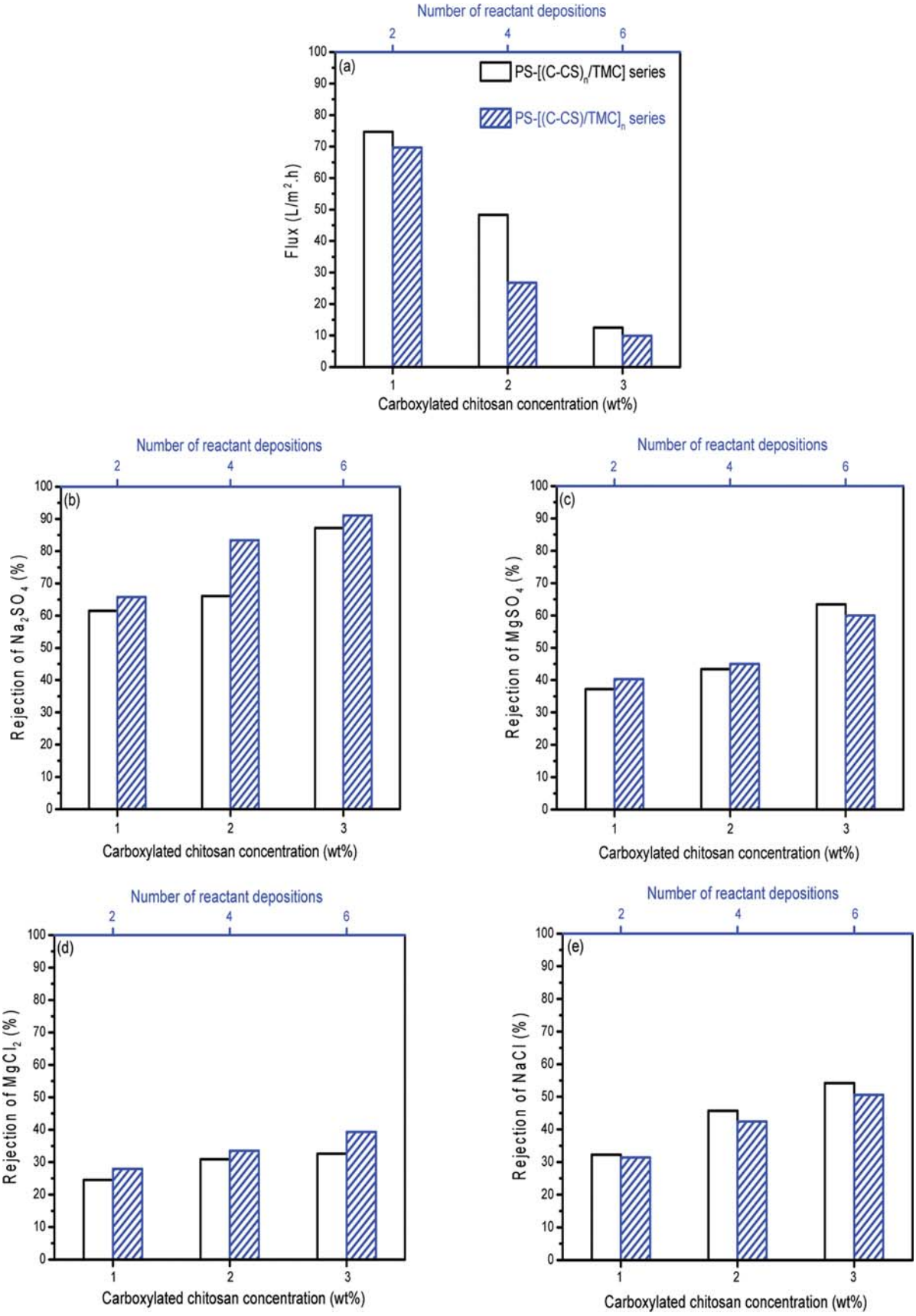

Fig. 11. A comparison of (a) permeation flux of pure water and salt rejection of (b) Na_2SO_4, (c) $MgSO_4$, (d) NaCl and (e) $MgCl_2$ in the two series of membranes (Testing conditions: 0.6 MPa gauge, 500 ppm salt concentration, 25 °C).

Table 5. Separation performance comparison of the membranes in this study to those of other polyester composite NF membranes

Membrane	Pure water permeability ($L/m^2 \cdot h \cdot MPa$)	Salt rejection (%)				Feed solution concentration (ppm)	Ref.
		Na_2SO_4	$MgSO_4$	$MgCl_2$	NaCl		
DMAP/TMC	12.0	96.3	83.9	28.8	58.7	1000	[12]
PE/TMC	13.4	98.1	67.9	26.4	49.7	1000	[17]
HPE/TMC	62.5	90.0	58.0	15.0	45.0	1000	[21]
Sericin/TMC	120	95.0	41.0	22.5	41.5	500	[22]
Tannic acid/TMC	137.5	49.5	50.5	19.5 ($CaCl_2$)	17.5	0.01 mol/L	[23]
Polydopamine/TMC	25	70	30	/	/	100	[24]
PS-[(C-CS)$_{3.5}$/TMC]	12.2	95.0	65.7	33.2	66.3	500	This study
PS-[(C-CS)/TMC]$_4$	11.2	97.0	67.4	49.7	54.7	500	This study

3. Effects of Operating Conditions on Dye Removal Efficiency

The single-layer polyesteramide membrane PS-[(C-CS)$_{1.0}$/TMC], which has a relatively loose structure, was used for the dye removal.

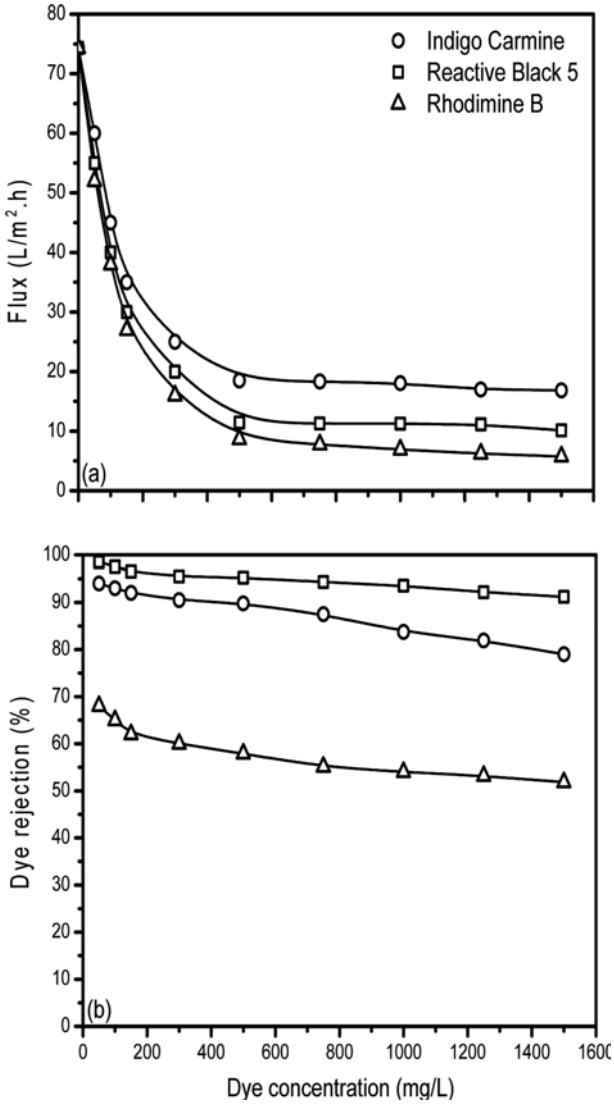

Fig. 12. Permeation flux (a) and dye rejection (b) of PS-[(C-CS)$_{1.0}$/TMC] membrane vary with the feed dye concentration (Testing conditions: 0.6 MPa gauge, 25 °C).

The permeation fluxes and dye removal rates of the three dye solutions under different feed dye concentrations are shown in Fig. 12. The permeation flux decreases dramatically with increasing dye concentration from 0 ppm to 300 ppm. Then, it decreases gently and even levels off with a further increase in the dye concentration to 1,500 ppm. The permeation fluxes of the three dye solutions are close to each other when the feed dye concentration was smaller than 200 ppm. The equilibrium flux of the three dye solutions appears to be in the order of indigo carmine>reactive black 5>rhodamine B. The dye removal rate gradually decreases by increasing the feed dye concentration to 1,500 ppm, and follows the order of reactive black 5>indigo carmine>rhodamine B.

This decline of the permeation flux and dye removal rate is mainly due to the increased osmotic pressure and the effect of the concentration polarization in the membrane separation process. As the feed dye concentration is increased, more dye molecules aggregate on the membrane surface, resulting in more dye molecules passing through the dense layer of the membranes. Similar results were also observed in other studies [35,36]. Moreover, the membrane has a relatively high rejection for the anionic dyes of reactive black 5 and indigo carmine due to its negatively charged surface. In addition to the charge properties, the large molecular weight of reactive black 5 is another reason for its highest rejection. Reactive black 5 is almost fully rejected (~99%) by the membrane under the low feed dye concentration. Even when the feed dye concentration increased to 1,500 ppm, the membrane still retained a high rejection of ~91% for reactive black 5. On the other hand, the cationic dye rhodamine B is easier to adsorb on the membrane surface due to the electrostatic attractions between the dyes and membrane surface. Its relatively low molecular facilitates the diffusion of the dye into the membrane pore, leading to pore blockage [6,35]. Thus, the membrane shows both the lowest permeation flux and removal rate for rhodamine B.

The effect of transmembrane pressure on the separation performance for the three dye solutions is shown in Fig. 13. The permeation fluxes of the three dye solutions increase linearly as the transmembrane pressure increases from 0.3 to 0.7 MPa. Generally, the permeation flux of the membrane is mainly determined by the porous structure of the membrane. The linear increase of the flux suggests that the membrane maintains an adequate amount of interconnected pores and remains a stable structure of the porous channels [37]. No structural deformation of the membrane was

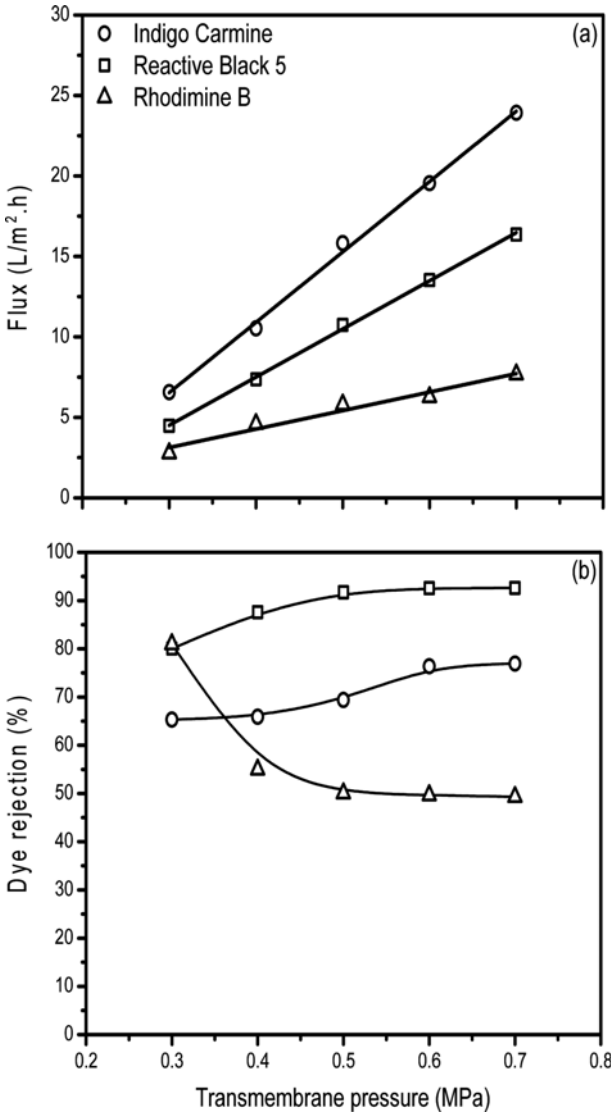

Fig. 13. Permeation flux (a) and dye rejection (b) of PS-[(C-CS)$_{1.0}$/TMC] membrane vary with the operating pressures (Testing conditions: 1,500 ppm dye concentration, 25 °C).

observed. The dye removal efficiency of reactive black 5 and indigo carmine increases slightly with increasing transmembrane pressure, while that of rhodamine B first decreases when the transmembrane pressure is increased to 0.5 MPa and then remains unchanged with the further increase of the transmembrane pressure up to 0.7 MPa. Two competing factors dictate the separation behavior of the solutes with an increase in the operating pressure. On the one hand, the dye molecules are sterically and electrostatically hindered while the water flux increases, leading to a "dilute effect" of the dye in the permeate. On the other hand, more dye molecules in the bulk solution transport toward the membrane surface by convection as the increased permeate flux, enhancing concentration polarization and subsequently reducing dye retention. For the reactive black 5 and indigo carmine, there is no significant concentration polarization on the feed side, and the "dilute effect" plays a dominant role in the separation, resulting in increased dye rejections. However, for rhodamine B, the increased pressure results in more dye than water permeating through the membrane because of the adsorption of the dye on the membrane surface. The dye removal rate stays the same as soon as the adsorption reached the equilibrium.

CONCLUSIONS

Single-layer and multiple-layer polyesteramide TFC NF membranes were fabricated by interfacial polymerization using carboxylated chitosan and trimesoyl chloride. Both the single-layer membrane PS-[(C-CS)$_{3.5}$/TMC] and the multiple-layer membrane PS-[(C-CS)/TMC]$_{4.0}$ show a high salt rejection of Na_2SO_4 (~95.0%). A more compact and thicker polyesteramide skin layer can be obtained by increasing either the reactant concentration or the number of reactant depositions. For enhancing the salt retention, the latter approach is more effective than the former. The multiple-layer polyesteramide membranes have a more negatively charged but less hydrophilic surface than the single-layer polyesteramide membranes. The single-layer polyesteramide membrane PS-[(C-CS)$_{1.0}$/TMC] with a relatively loose structure shows >90% removal rate for the reactive black 5 anionic dye, even under a high feed dye concentration of 1,500 ppm. It is found that the carboxylated chitosan/TMC membranes with good separation performance and durability could be potentially used in waste water treatment. The membrane PS-[(C-CS)$_{1.0}$/TMC] is recommended for dye removal and the membrane PS-[(C-CS)$_{3.5}$/TMC] or PS-[(C-CS)/TMC]$_{4.0}$ is a good choice for water softening.

ACKNOWLEDGEMENT

The authors gratefully acknowledge the financial support by the Research Foundation of Zhejiang Educational Committee (Y201840390), Research Foundation from Hangzhou Dianzi University (KYS205618007) and the National Nature Science Foundation of China (NNSFC) (Grant No. 21676256).

REFERENCES

1. O. Labban, C. Liu, T. H. Chong and J. H. Lienhard V, *J. Membr. Sci.*, **521**, 18 (2017).
2. Y. Zhao, N. Li and S. Xia, *Compos. Sci. Technol.*, **132**, 84 (2016).
3. X. Q. Cheng, Z. X. Wang, Y. Zhang, Y. Zhang, J. Ma and L. Shao, *J. Membr. Sci.*, **554**, 385 (2018).
4. J. Garcia-Ivars, L. Martella, M. Massella, C. Carbonell-Alcaina, M.-I. Alcaina-Miranda and M.-I. Iborra-Clar, *Water. Res.*, **125**, 360 (2017).
5. K. Nath, H. K. Dave and T. M. Patel, *Trends. Food Sci. Technol.*, **73**, 12 (2018).
6. G. Han, T.-S. Chung, M. Weber and C. Maletzko, *Environ. Sci. Technol.*, **52**, 3676 (2018).
7. G.-E. Chen, Y.-J. Liu, Z.-L. Xu, Y.-J. Tang, H.-H. Huang and L. Sun, *RSC. Adv.*, **5**, 40742 (2015).
8. G.-E. Chen, Y.-J. Liu, Z.-L. Xu, D. Hu, H.-H. Huang and L. Sun, *J. Appl. Polym. Sci.*, **132**, 42345 (2015).
9. D. Hu, Z.-L. Xu, Y.-M. Wei, S. Cao, W.-D. Chen and X.-H. Qian,

Sep. Sci. Technol., **48**, 554 (2013).
10. F. Xiao, B. Wang, X. Hu, S. Nair and Y. Chen, *J. Taiwan. Inst. Chem. E.*, **83**, 159 (2018).
11. M. Wu, T. Ma, Y. Su, H. Wu, X. You, Z. Jiang and R. Kasher, *J. Membr. Sci.*, **544**, 79 (2017).
12. R. Zhang, S. Yu, W. Shi, W. Wang, X. Wang, Z. Zhang, L. Li, B. Zhang and X. Bao, *J. Membr. Sci.*, **542**, 68 (2017).
13. S. Yang, H. Zhen and B. Su, *RSC. Adv.*, **7**, 42800 (2017).
14. Y. Hai, J. Zhang, C. Shi, A. Zhou, C. Bian and W. Li, *J. Membr. Sci.*, **520**, 19 (2016).
15. M. N. A. Seman, M. Khayet and N. Hilal, *Desalination*, **273**, 36 (2011).
16. K. H. Mah, H. W. Yussof, M. N. A. Seman and A. W. Mohammad, *IOP Conf. Ser.: Mater. Sci. Eng.*, **162**, 012037 (2016).
17. J. Cheng, W. Shi, L. Zhang and R. Zhang, *Appl. Surf. Sci.*, **416**, 152 (2017).
18. D. Wu, Y. Huang, S. Yu, D. Lawless and X. Feng, *J. Membr. Sci.*, **472**, 141 (2014).
19. M. Liu, Y. Zheng, S. Shuai, Q. Zhou, S. Yu and C. Gao, *Desalination*, **288**, 98 (2012).
20. L. Li, B. Wang, H. Tan, T. Chen and J. Xu, *J. Membr. Sci.*, **269**, 84 (2006).
21. X. Wei, X. Kong, J. Yang, G. Zhang, J. Chen and J. Wang, *J. Membr. Sci.*, **440**, 67 (2013).
22. C. Zhou, Y. Shi, C. Sun, S. Yu, M. Liu and C. Gao, *J. Membr. Sci.*, **471**, 381 (2014).
23. Y. Zhang, Y. Su, J. Peng, X. Zhao, J. Liu, J. Zhao and Z. Jiang, *J. Membr. Sci.*, **429**, 235 (2013),.
24. J. Zhao, Y. Su, X. He, X. Zhao, Y. Li, R. Zhang and Z. Jiang, *J. Membr. Sci.*, **465**, 41 (2014).
25. Y. Huang, J. Sun, D. Wu and X. Feng, *Sep. Purif. Technol.*, **207**, 142 (2018).
26. Y.-J. Tang, L.-J. Wang, Z.-L. Xu and H.-Z. Zhang, *J. Polym. Res.*, **25**, 118 (2018).
27. X.-H. Ma, Z. Yang, Z.-K. Yao, Z.-L. Xu and C. Y. Tang, *J. Membr. Sci.*, **525**, 269 (2017).
28. M. Dash, F. Chiellini, R. M. Ottenbrite and E. Chiellini, *Prog. Polym. Sci.*, **36**, 981 (2011).
29. X. Kong, Y. Zhang, S.-Y. Zeng, B.-K. Zhu, L.-P. Zhu, L.-F. Fang and H. Matsuyam, *J. Membr. Sci.*, **518**, 141 (2016).
30. S. Ilyas, J. Grooth, K. Nijmeijer and W. M. de. Vos, *J. Colloid Interface Sci.*, **446**, 386 (2015).
31. W. Cheng, C. Liu, T. Tong, R. Epsztein, M. Sun, R. Verduzco, J. Ma and M. Elimelech, *J. Membr. Sci.*, **559**, 98 (2018).
32. Y.-J. Tang, Z.-L. Xu, S.-M. Xue, Y.-M. Wei and H. Yang, *J. Membr. Sci.*, **541**, 483 (2017).
33. M. Liu, D. Wu, S. Yu and C. Gao, *J. Membr. Sci.*, **326**, 205 (2009).
34. N. Dizge, R. Epsztein, W. Cheng, C. J. Porter and M. Elimelech, *J. Membr. Sci.*, **549**, 357 (2018).
35. C. Zhao, B. Yang, J. Han, Y. Meng, L. Yu, D. Hou, J. Wang, Y. Zhao, Y. Zhai, S. Wang and X. Sun, *Appl. Surf. Sci.*, **453**, 502 (2018).
36. M. Peydayesh, T. Mohammadi and O. Bakhtiari, *Sep. Purif. Technol.*, **194**, 488 (2018).
37. C. Zhijiang, Z. Cong, X. Ping, G. Jie and Z. Kongyin, *J. Mater. Sci.*, **53**, 14801 (2018).